Pergamon

Phys. Chem. Earth (C), Vol. 24, No. 1–3, pp. 189–202, 1999

1464-1917/99/$—see front matter

PII: S1464-1917(98)00028-2

The Physics of Substorms as Revealed by the ISTP

K. Papadopoulos[1], C. Goodrich[1], M. Wiltberger[1], R. Lopez[1] and J. G. Lyon[2]

[1]Departments of Physics and Astronomy, University of Maryland, College Park, Maryland, U.S.A.
[2]Department of Physics, Dartmouth College, Hanover, New Hampshire, U.S.A.

Received 11 November 1997; accepted 6 March 1998

Abstract

Spacecraft and ground data combined with multiscale computer models developed by the ISTP program are providing a new and coherent understanding of the magnetospheric substorms and storms. Global MHD simulations that include ionospheric response are dynamically driven by upstream satellite data and allow for direct comparison with the field and flow quantities measured by magnetospheric satellites, ground data and images from the POLAR satellite. Through the combined analysis of the simulations and observations, the first unified picture of a substorm from the magnetospheric and ionospheric viewpoint is currently emerging. Here we use MHD simulations of two particularly well observed and analyzed events to explore the factors that trigger and organize the substorm elements into a coherent entity. The first event — March 9, 1995 — produces clear evidence that impulsive penetration of a large electric field in the vicinity of -8 to -10 R_E, possibly associated with magnetosonic energy focusing, acts as a trigger for substorm initiation. It is the element that connects the ionospheric to magnetospheric substorm. Particularly impressive is the timing of the chain of events and indices observed on the ground and their proxies computed in the simulation. This simulation is complemented by a "theoretician's" simulation, a step function transition of the IMF from northward to southward, which clarifies the physics of energy penetration into the magnetosphere and demonstrates Poynting flux focusing in the near earth tail. The second event — January 10–11, 1997 — was driven by the impact of a magnetic cloud in the magnetosphere. It induced major disturbances in the magnetosphere and the groundand resulted in the loss of a geosynchronous ATT satellite. It is a simulation "tour de force" and used continuous upstream data over 36 hours as input. The results provide a graphical and fascinating view of the global magnetospheric and tail response to a magnetic cloud impinging upstream, illustrate the importance of dynamics and indicate that pressure impulses play a key role in providing the coherence required for substorms.

1. Introduction

With the launch of the POLAR satellite, the major space based components of the ISTP program are in place and producing a continuous stream of data. The global theory and simulation program, a GGS component, developed a series of computational sequences specifically designed to receive data from the ISTP spacecraft and from the ground investigations. These sequences constitute the framework within which the ISTP measurements, taken in diverse locations in space and the ground, are globally integrated, classified and interpreted. In this paper we present three examples of this work, conducted at the University of Maryland, addressing scientific issues related to the physics of storms and substorms (Akasofu, 1968). These examples use a 3–D MHD code, advanced visualization tools, and spacecraft and ground data, to develop an integrated picture of the geospace dynamics during active periods. The first example is a simulation of an isolated substorm. The event occurred on March 9, 1995, and due to its extensive ground and space coverage, is an excellent test of model and data comparison. The second example is a theoretician's example, based on simple solar wind input having a north to south IMF transition. These results illustrate the basic physical processes involved in the more realistic and complex first example. The third example is a simulation of the magnetic storm involving a series of substorms that occurred on January 10–11, 1997, known as the storm that coincided with the failure of Telstar 401ATT satellite. This simulation is an excellent example of long time (> 36

"*Correspondence to:*" K. Papadopoulos, University of Maryland, Physics Department, College Park, MD 20742

hours) global dynamics. Preceding the discussion of the examples is a brief description of the 3D MHD model used in the simulations.

2. The Lyon-Fedder-Mobbary (LFM) code

The simulations described in Sect. 3 were performed using the Lyon-Fedder-Mobarry (LFM) code and analyzed with visualization software developed at the University of Maryland. The LFM code (Fedder and Lyon, 1995) has two tightly coupled modules. The first module is a 3D MHD code that simulates the solar wind-magnetosphere interaction. This module uses a logically spherical grid deformed to be nearly cylindrical with radius 60 R_E and axis length 300 R_E. The long axis of the cylinder is tilted away from the Earth-Sun line to approximate the position of the Earth's dipole moment at the event time. The computational grid is designed to placing maximum resolution at critical locations. A diffuse solar wind matching condition is used along the outer edges of the computational grid, thereby allowing use of time dependent solar wind parameters, as input conditions. A simple supersonic outflow condition is used at the far tail boundary, x = -300 R_E. The second module represents the lower boundary, the ionosphere. This module is a 2D height integrated electrostatic model, that solves Poisson's equation

$$\nabla\Sigma \nabla \Phi = J_{\|}$$

where Φ is the ionospheric potential, Σ the conductivity tensor and $J_{\|}$ the field aligned current. The conductivity tensor has both Petersen and Hall components, whose values are spatially varying with prescriptions dependent on the electron precipitation and SUV (Fedder and Lyon, 1995). The ionospheric model is coupled to the inner boundary of the MHD module, located typically at 2–3 R_E, by a line tying matching condition (Coroniti and Kennel, 1973). The field aligned currents ($J_{\|}$) are calculated from the magnetic field data on the inner edge of the MHD model and used in conjunction with the model of Σ to determine the potential Φ in the ionosphere. The potential is then mapped back to the MHD boundary, where it is used to calculate the electric field necessary to update Faraday's law.

3. Examples

3.1 Isolated substorm — March 9, 1995

The first example presented is that of a substorm that occurred in the early hours of March 9, 1995. This substorm was initially identified by Allan Rodgers of the British Antarctic Survey, who compiled an extensive set of detailed ground data. This is a particularly good example because followed an extended period northward IMF ($\gtrsim$ 8 hours), in which the magnetosphere had settled into its "ground state". The input to the code was provided by the upstream WIND measurements shown in Fig. 1. Note that pressure pulse of 0230 UT followed by the southward turning of the IMF at 0237 UT. (The times shown in Fig. 1 are shifted by 54 minutes corresponding to the propagation time from the Wind location to the code boundary located at 30 R_E). Table I shows the observational morphology of the event. The results of the LFM simulations are shown in Figs. 2–4. A movie version of the simulations that displays the dynamics involved can be found in http://www.spp.astro.umd.edu. The initial state is shown in Fig. 2a at 0300 UT. The translucent surface, which corresponds to the surface of the last closed lines, is consistent with the northward IMF configuration. Figures 2b and 2c refer to times 0456 and 0511 UT. From Table I we see that this is the period that ground based and satellite measurements detected substorm signatures. Notice that appearance of hot plasma (orange surface) in the vicinity of 10 R_E. A complementary diagnostics is shown in Fig. 3. It shows the value of the electric field at the three instants of time.

Key items of interest first appear in Fig. 3b. A reconnection region has been formed near 30 R_E, while an enhanced electric field appeared in the inner tail region ($<$ 10 R_E). This field is far from the reconnection region which occurs farther down the tail. The animation shows that after the electric field impulse reached the center of the plasma sheet, it launched a tailward propagating signal. When this signal reached the reconnection region, it increased significantly its rate, as seen from the flows shown in Fig. 3c. We associate the impulsive field penetration at 0456 UT with the focusing effect (Papadopoulos et al., 1993). This will be addressed in the second example (Sect. 3.2). Detailed comparison of the code results with the IMP and Geotail observations shows good agreement (Lopez et al., 1997). This view of the magnetospheric substorm is complemented with the view of the ionospheric substorm shown in Fig. 4. Figure 4a shows the simulated polar cap flux with the polar cap (defined as the open-closed field line boundary), while Fig. 4b the polar cap boundaries along the noon and midnight meridians. At 0335 UT the polar cap began to grow. Growth continued till 0454 UT, when it began to shrink the rate increased dramatically at 0503 UT and continued until 0530 UT. Figure 4c shows a synthetic AL computed in the code on the basis of the ionospheric currents. Its behavior is consistent with substorm onset at 0454 UT and intensification at 0508. The timing shown in Figs. 4, is in excellent agreement with the CANOPUS data (Lopez et al., 1997). By comparing the view of the magnetospheric substorm (Figs. 2 and 3), with the ionospheric substorm (Figs. 4) we note the mapping of the one to the other. Furthermore, the electric field spike penetrating the 10 R_E region at 0554 UT seems to trigger the substorm as well as coupling the magnetospheric to the ionospheric substorm. Details of these will be discussed elsewhere.

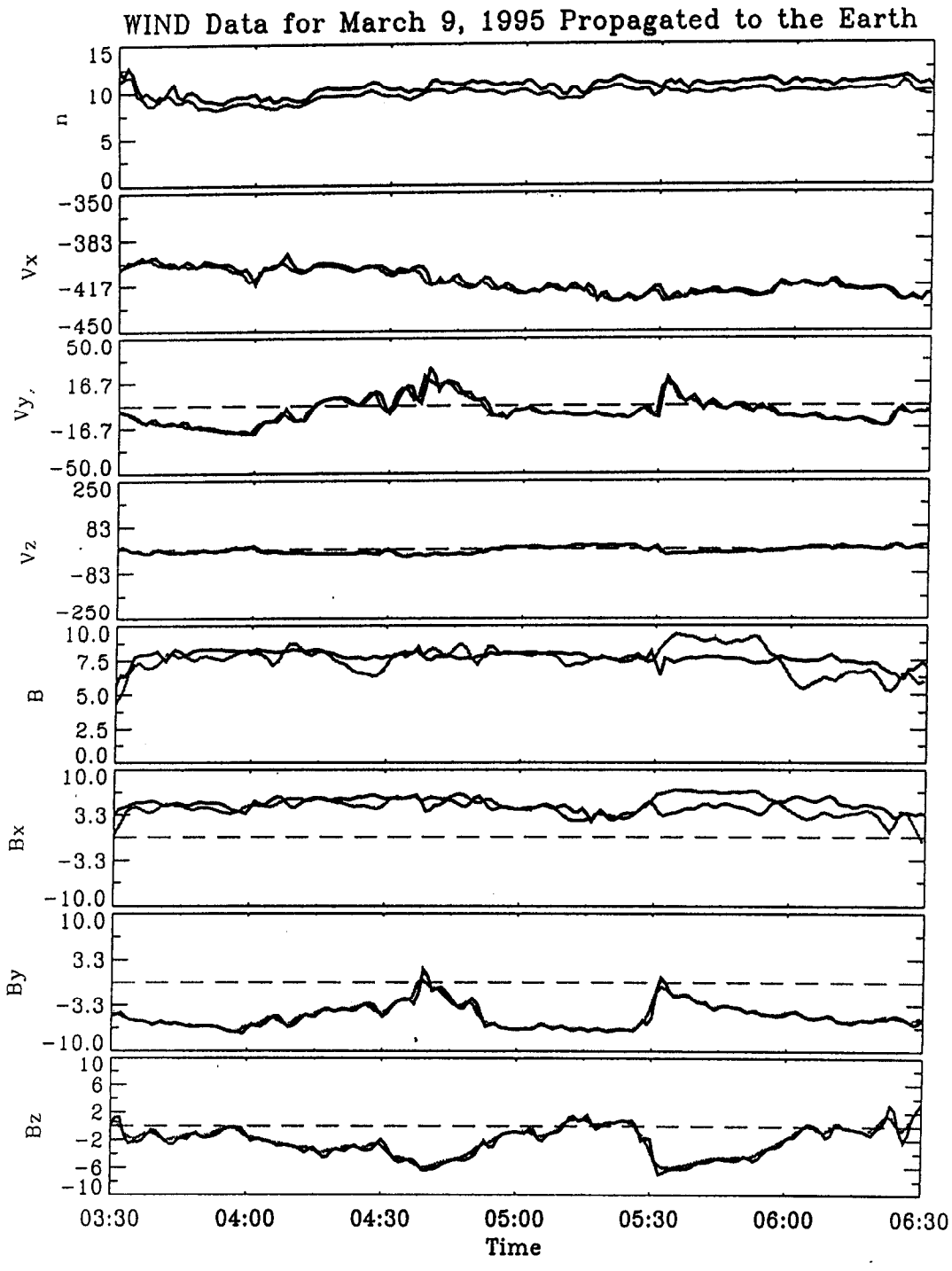

Fig. 1. WIND measurements used as input to the MHD simulations for March 9, 1995 event. The dotted line shows the measurements, while the solid line the smoothed data used in the code, including adjustments to preserve $\nabla \cdot \mathbf{B} = 01$.

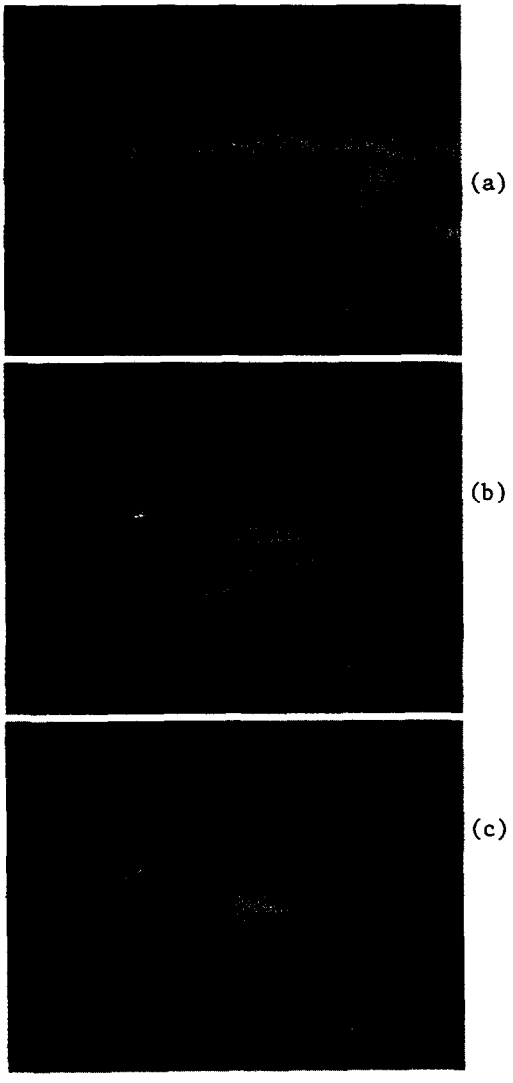

Fig. 2. Results of simulations at three diffrent times in the noon-meridien plane. On the left of each figure is the clock angle of the IMF, and the arrow is proportional to the ram pressure (logarithmic scale). The density is color coded, while the arrows are flow vectors. The transluscent surface represents the surface of the last closed magnetic field lines. (a) 03:10:51 UT (b) 04:56:55 UT (c) 05:11:40 UT.

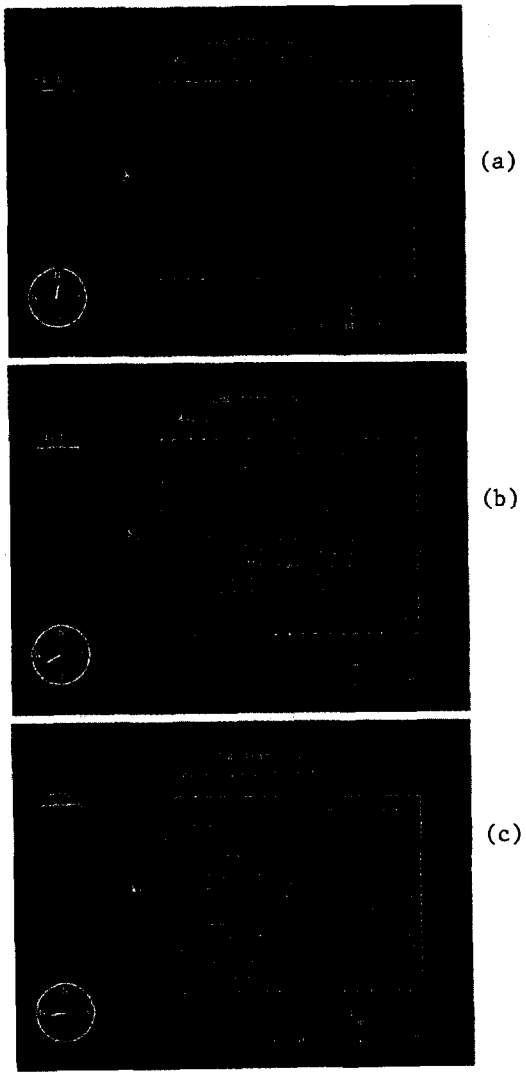

Fig. 3. Same as Figure 2, but the color plots represent the value of the electric field. Notice the enhanced electric field at the substorm time (04:56:55) in the vicinity of -10 R_E, as well as its penetration beyond -10 R_E at 05:11:40.

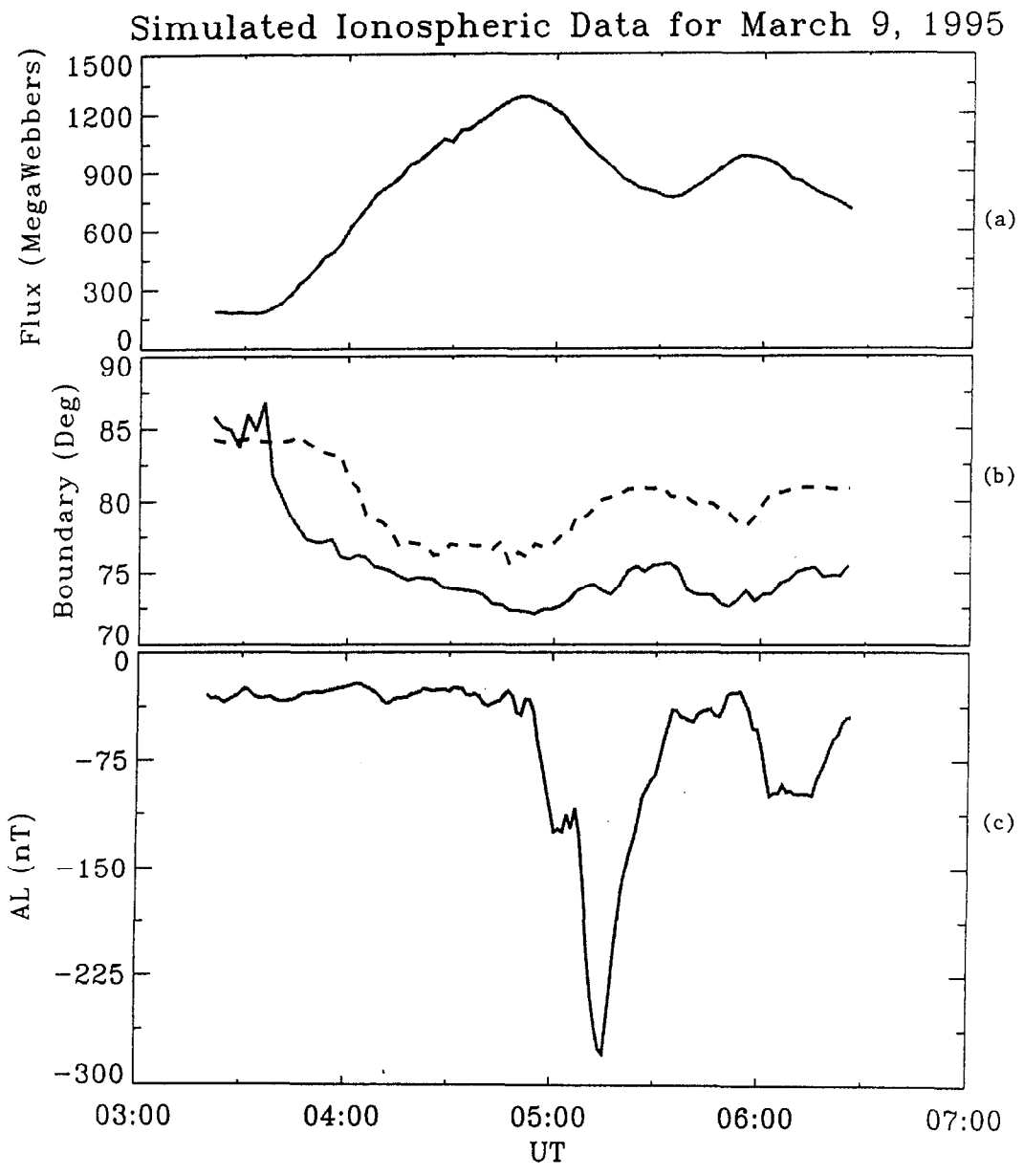

Fig. 4. Ionospheric data as measured in the simulation; (a) simulated polar cap flux, (b) location of polar cap boundaries, (c) synthetic AL.

Table 1
Sequence of events - 9 March 1995

Time UT	Event	Diagnostic
0230	Start of pressure pulse (Ne rises by 50%)	Wind
0237	Southward turning of the IMF	Wind
~0330	Pressure pulse first seen on dayside, and then globally	Magnetometers
~0340	DP2 current system increases - growth phase starts	Magnetometers HF radars DMSP
0456	Geotail moves from N to S tail lobe	Geotail
0457	Flux of energetic particles reduces rapidly at L = 6.6	LANL spacecraft near magnetic midnight
0500	Bz begins to diminish at -30 R_E	IMP-8
0501	Pi2 seen at mid-latitudes	Ottawa and other magnetometers
0503	Vy oscillates with Pi2 period	Geotail
0504	Dipolarisation begins at Geotail	Geotail
0505	Flux of energetic particles begins to increase very rapidly at L = 6.6 Bz begins to recover at -30 R_E	LANL spacecraft near magnetic midnight IMP-8
~0505	Baylike disturbances seen in Greeland centred at Narsarssuaq	Magnetometer
0520	Injection at geostationary orbit	LANL spacecraft near magnetic midnight
0530	Second P2 Large intensification in East Greenland and IMAGE Large intensification observed over Canada Small intensification seen over west Greenland	Magnetometers

3.2 Southward IMF turning — a theoretician's simulation

The second example to be presented is a theoretician's simulation whose objective is to elucidate key aspects of the physics previously described by initiating the simulation with a well defined symmetric driver.

This particular simulation run is discussed in Lyon and Fedder (1997). The solar wind parameters used were: density n = 5 cm^{-3}, velocity U = 400 km/sec, Mach number M = 10, and magnetic field magnitude |B| = 5 nT. The simulations sequence of interest here starts with northward IMF (B_z = 5nT). This state was established holding B_z constant at this value for about 2 hours of simulated magnetospheric time [Fedder and Lyon, 1997]. The IMF was the abruptly changes to southward (B_z = -5 nT) at the upstream boundary and kept at this value throughout the simulation completing an idealized substorm scenario. Throughout the run the temporal resolution was under one second, allowing for unambiguous propagation of fast magnetosonic waves in the mesh.

As noted in Lyon and Fedder [1997] the simulation shows a striking resemblance to the "typical" substorm including growth and expansion phase. Figure 5 (taken from the above paper) summarizes their results and provides a timeline for the discussion of our results; time is given from the arrival of the field transition at the subsolar point of the magnetopause. Shown is the cross polar cap potential and its time derivative during the substorm sequence. The time derivative shows two clear impulses. The first, indicating the start of the growth phase, occurs at 10–20 min. The second impulse, indicating the expansion phase, occurs at 60 — 80 min, and is associated with the development of a neutral line and strong reconnection in the tail at -23 R_E. We refer the reader to Lyon and Fedder [1997] for further details.

To study the flow of electromagnetic energy and momentum during the simulation substorm sequence, we follow the propagation of the Poynting flux $\mathbf{S} = c/4r\ \mathbf{E}\times\mathbf{B}$ momentum, computed using the total instantaneous values for **E** and **B**. Thus **S** represents the total Poynting flux; we have not attempted the very difficult task of separating the contributions from plasma convection of static fields — such as in the upstream solar wind -from propagation of dynamic field structures including magnetosonic waves. However, we can compare the directions of the Poynting flux and plasma flow to determine qualitatively the relative importance of these contributions. Both **S** and the plasma velocity V in the north-south plane are shown in the following figures. White streamlines originating at source points on a north -south line at X = 20 R_E show the flow of **S**; blue arrows show the direction and magnitude of V. As indicators of the magnetospheric state at these times, we also show — in the north-south- plane - a color map of the log of the plasma pressure and (in yellow) the boundary of the closed field region.

Figure 6a shows the results before the transition from northward to southward IMF occurred, about 10 minutes before the events indicated in Fig. 5. At this point, the IMF had been held northward for over two hours, and the closed region of the tail has expanded to about 100 R_E downstream; however the closed field boundary is still in the tail lobe region inside the magnetopause. The white streamlines indicate the flow of **S** starting at points in the north-south plane at X = 20 R_E, where **S** represents the convection of the IMF by the solar wind. At the bow shock, **S** is deflected toward the magnetopause, and propagates roughly perpendicular to the plasma flow. At the magnetopause, indicated by the sharp drop in plasma pressure in the figure, **S** is essentially deflected onto the magnetopause surface downstream, with the exception of a small fraction that encounters reconnection sites at high latitudes. It is clear that the magnetopause is a barrier to both electromagnetic and plasma momentum and energy

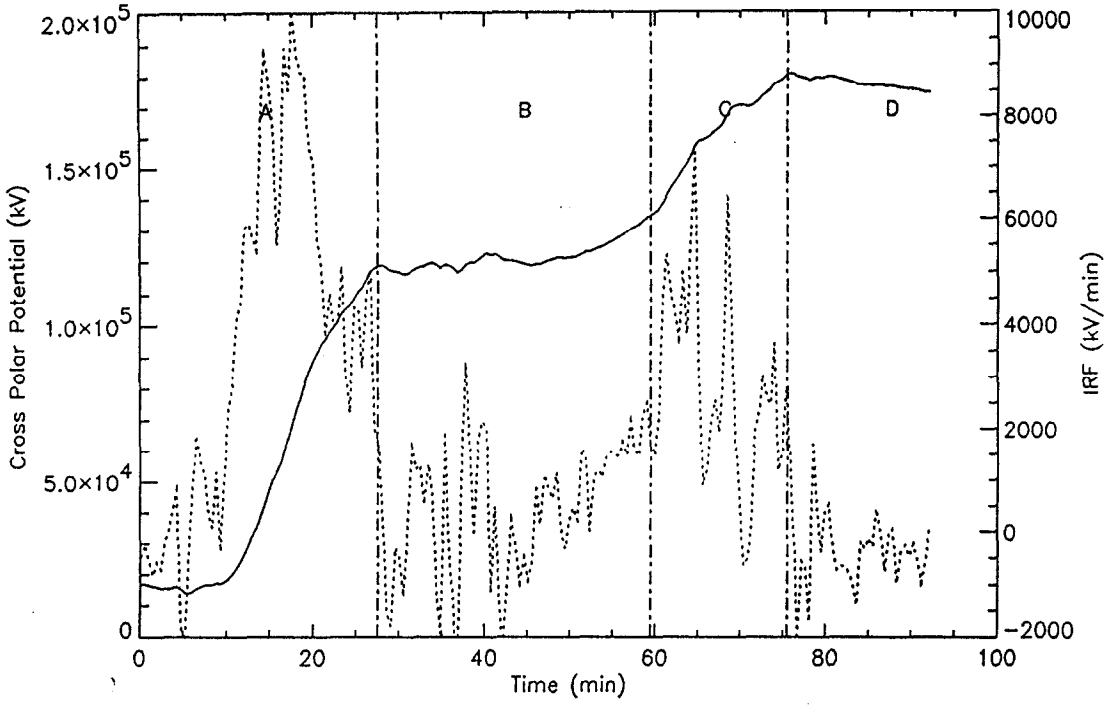

Fig. 5. Polar cap potential and its derivative as a function of time during the simulation of Sect. 3.2 (Fedder and Lyon 1995).

flow, corresponding to the classic picture of the closed magnetosphere. Further, the propagation of S transverse to the plasma flow requires time dependent effects, which can only be produced in dynamic models such as the MHD code. From the apparent skimming of S along the downstream magnetopause, one can also speculate that surface waves could be excited in this region leading to micropulsations.

The behavior for S changes dramatically during the substorm growth phase. Figure 6b shows the results for t = 17.10 min., when the field transition had been convected to about X = -18 R_E. Here we have restricted the trace of S to source points with Z > 10 R_E to eliminate streamlines which impinge on reconnection sites S now at low latitudes for southward IMF; these streamlines are diverted onto the magnetopause surface and down into the ionosphere in tangled trajectories that obscure the results in the near Earth tail.

The flow of S is similar to that in Fig. 6a until the magnetopause is reached. Now S easily penetrates the magnetopause upstream of the field transition (clearly indicated by the confused tangle of streamlines to the upper right of the figure) and appears to be focused toward the central plasma sheet around X = -6 to -10 R_E. In contrast no significant change can be seen in the plasma flow nor the tail magnetic field structure from the northward IMF configuration in Fig. 6a, indicating the transport of S into and within the magnetotail is primarily dynamic propagation rather than plasma convection of field flux. This conclusion is further supported by noting the expansion of the closed field boundary to near the magnetopause, which shows the magnetic field was being transported outward, not inward, during the period between Fig. 6a and Fig. 6b. These results are, to our knowledge, the first clear indication of how solar wind momentum penetrates into the magnetosphere and reaches the near Earth tail. They are also generally consistent with the expectations of the simplified lens model of Papadopoulos et al. [1993].

Figure 6c shows the situation at t = 55.08 min., just before the beginning of the substorm expansion phase. At this point, the focusing pattern for S has been fully disrupted. Again the streamlines of S approach the magnetopause much as before, but are diverted duskward as they move down toward the plasma sheet and then antisunward. Note the viewpoint in Figure 6c has been rotated by about 45 degrees duskward to make this +Y diversion more visible. This diversion is sufficient to keep S from entering the now contracting closed field boundary in the tail and appears to be associated with the initial development of a neutral line apparent at about X = -23 R_E. Note that the

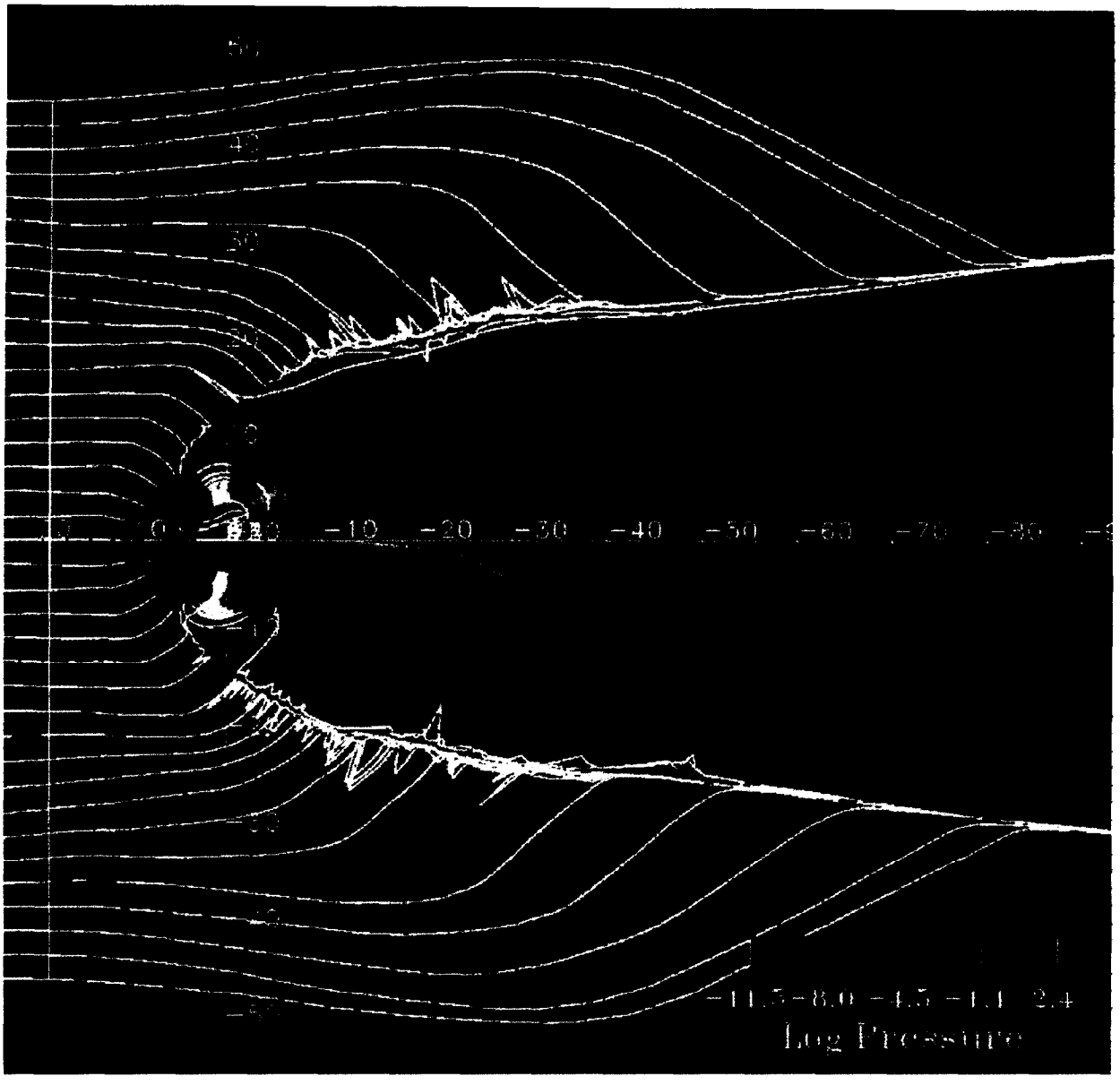

Fig. 6. Meridional plane showing the plasma pressure (logscale), the plasma velocity vector (blue) and the Poynting vector streamlines (white). The yellow line represents the closed magnetic field boundary. The field turns southward at t = 0.

(a) t = -10 minutes
(b) t = 17.1 minutes
(c) t = 55.08.

Notice the penetration and focusing of S in (b) and the loss of focusing in (c).

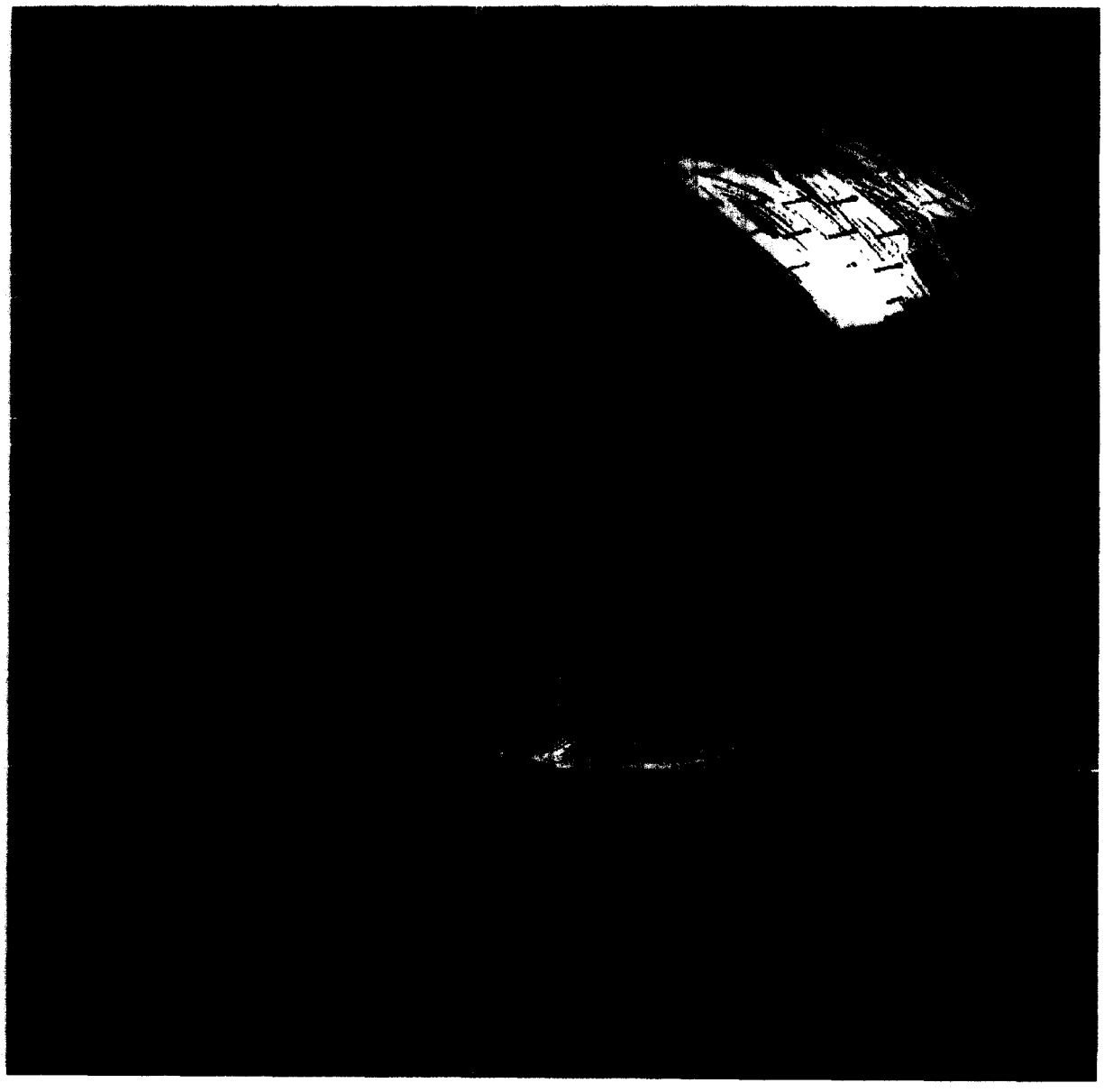

Fig. 6b

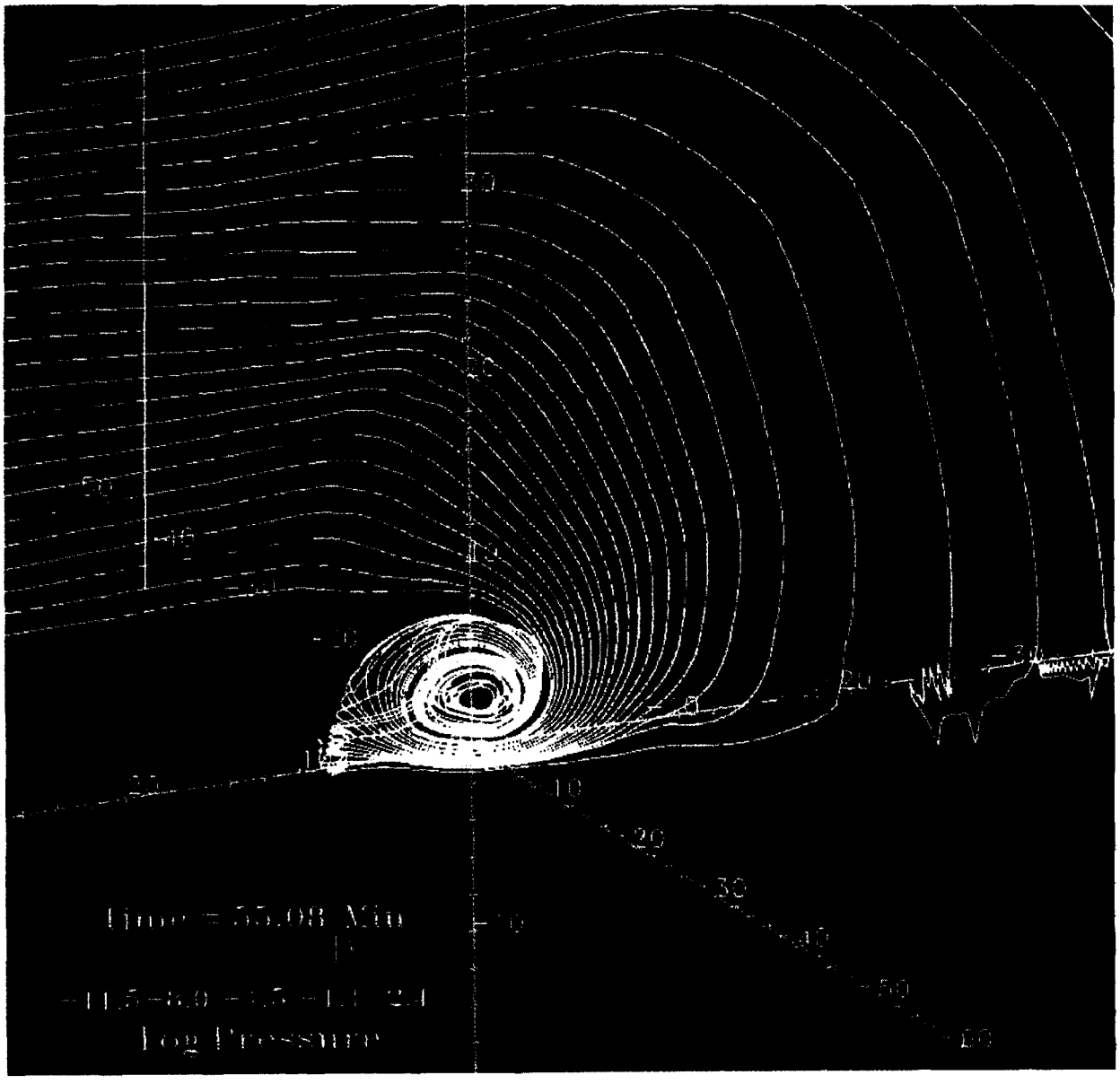

Fig. 6c

streamlines pass the boundary on the duskward side and outside of the closed field region. The neutral line has not yet fully formed; though moving inward, and beginning to pinch in at the distance, the closed field boundary about 12 R_E equatorial plane. However, there are enhanced plasma flows associated with neutral line formation in the appropriate direction to divert S. In any case, the focusing of S started by with the southward turning of the IMF is ended at the start of the substorm expansion phase.

In this simulation we followed the evolution of a substorm by tracing the flow of the Poynting flux S, and contrasting it to the plasma flow, we found that the entry of electromagnetic flux is strongly linked to substorm phase. For northward IMF, before the transition to southward IMF that initiated the substorm, we found that the Poynting flux did not enter the magnetotail; it was diverted onto the magnetopause surface and propagated downstream. Thus for northward IMF the magnetopause is a barrier to the entry of both electromagnetic and plasma energy and momentum. During the substorm growth phase, when reconnected magnetic flux is being added to the tail, we find the Poynting flux easily penetrates the magnetopause and focuses toward the near Earth plasma sheet at X = -6 to $-10\,R_E$ and with $|Z| < 3\,R_E$ and $|Y| < 5\,R_E$. Finally the focusing is disrupted at the beginning of the substorm expansion phase, apparently by plasma flows associated with the formation of a reconnection region further downstream at X = -23 R_E.

The results provide a physical explanation of the observational correlation of the near Earth plasma sheet with the strongest signature of the substorm growth phase Lopez and Lui (1990), Lopez et al. (1991), Lui et al. (1990). An important result of our investigation is that the dominant energy and momentum transport process during the substorm growth phase is electromagnetic rather plasma in nature. This simulation provides a natural interpretation of the electric field penetration noted in Sect. 3.1.

3.3 Complex storm — January 10–11, 1997

The last example is that of a complex storm that took place on January 10–11, 1997, known as the storm that coincided with the failure of the Telstal 401 ATT satellite. The simulation was initiated using upstream wind data, as in example 3.1. Forty-eight hours of real time was simulated. Space limitations do not allow more than a superficial description of this complex event, which was characterized by extreme dynamic changes in the tail and seldomly demonstrated stationary. This example is best appreciated by viewing it in its animation form (http://www.spp.astro.umd.edu). The event began January 10, 1997, 01.00 UT, with the arrival of a shock wave, which preceded the arrival of a magnetic cloud. The simulation was initiated several hours earlier. A period of substorm activity occurred between 0300 and 0500 UT, which was observed in the ionosphere and can be clearly seen in the simulation video. The magnetic cloud arrived between 0500 and 0600 UT. Significant substorm activity can be seen in the simulation video, especially between 0500 — 0600 UT and 1100 — 1200 UT, times associated with southward IMF. However, continuous activity occurred in between these times, with the magnetotail showing extreme dynamic motion. An example of the dynamic activity can be seen in Fig. 7(a-c) which, except for the flow vectors, has the same format as Fig. 2. The time shown spans a substorm which occurred between 0309–0312 UT. The radical change of the magnetospheric configuration seen in Figs. 7b and 7c, is very impressive. Particularly noteworthy is the correlation of the substorm occurance with relaxation of the pressure exerted on the magnetopause (upper arrow in left hand side of figures). In fact similar correlations appear throughout the run.

The solar wind input changed significantly on January 11 between 0000 and 0300 UT with the appearance of a dense plasma filament ($n \gtrsim 160$ #/cm^3), which followed the cloud passage. The resulting enormous increase in the solar wind ram pressure compressed the entire magnetosphere, and moved the dayside magnetopause well within the geosynchronous orbit by 0150 UT. This is clearly evident in Fig. 8 which shows the plasma density in the ecliptic plane at 0115 and 0150 UT; the black line indicates geosynchronous orbit. Representative open (white) and closed (orange) magnetic field lines are shown as well. Note that we have doubled the radius of the earth to make it easily visible in the figure.

4. Summary and conclusions

We presented above brief descriptions intended to describe the methodology used in the ISTP program to advance our understanding of substorms. A key element in the analysis is the LFM code, which is most often initiated by actual upstream data as measured experimentally. The first example was an excellent code validation test. It reproduced the timing and key features of the isolated substorm, seen in both ground and satellite observations. It, furthermore, allowed us to identify the important role of the electric field spike in triggering the substorm as well as coupling the ionospheric and magnetospheric responses. The second example, by using a symmetric configuration and a controlled step function IMF transition, allowed identification of the dominant energy penetration form into the magnetosphere and confirmed the concept of Poynting flux focusing. The sheer volume of data which exceeds 7 Gbs and is currently analyzed was a major problem in discussing the last example in any detail. We chose to present two figures indicative of the extreme dynamics and refer the interested reader to the animated form. Details will appear elsewhere.

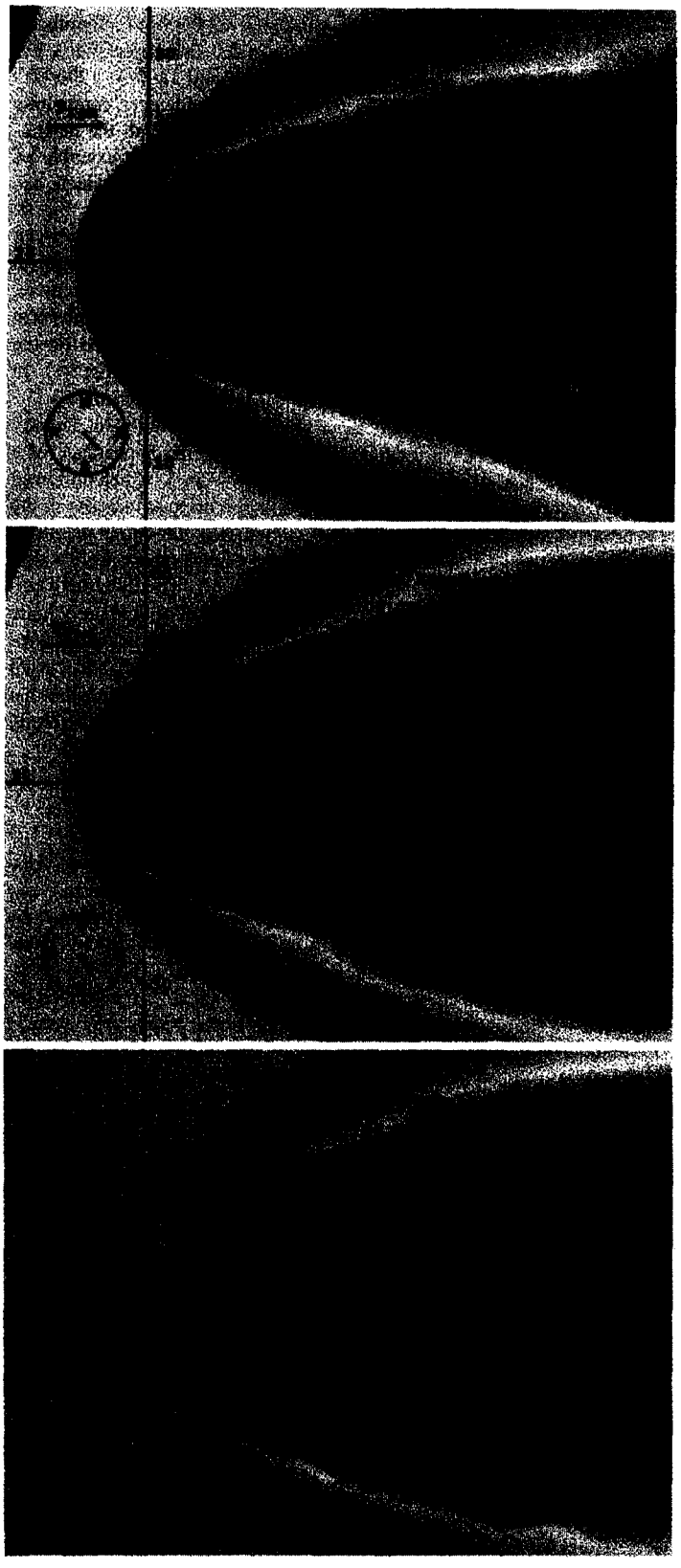

Fig. 7. Dynamic response of the magnetosphere before and during the substorm that occured between 03:00–03:30 UT on January 10, 1997.

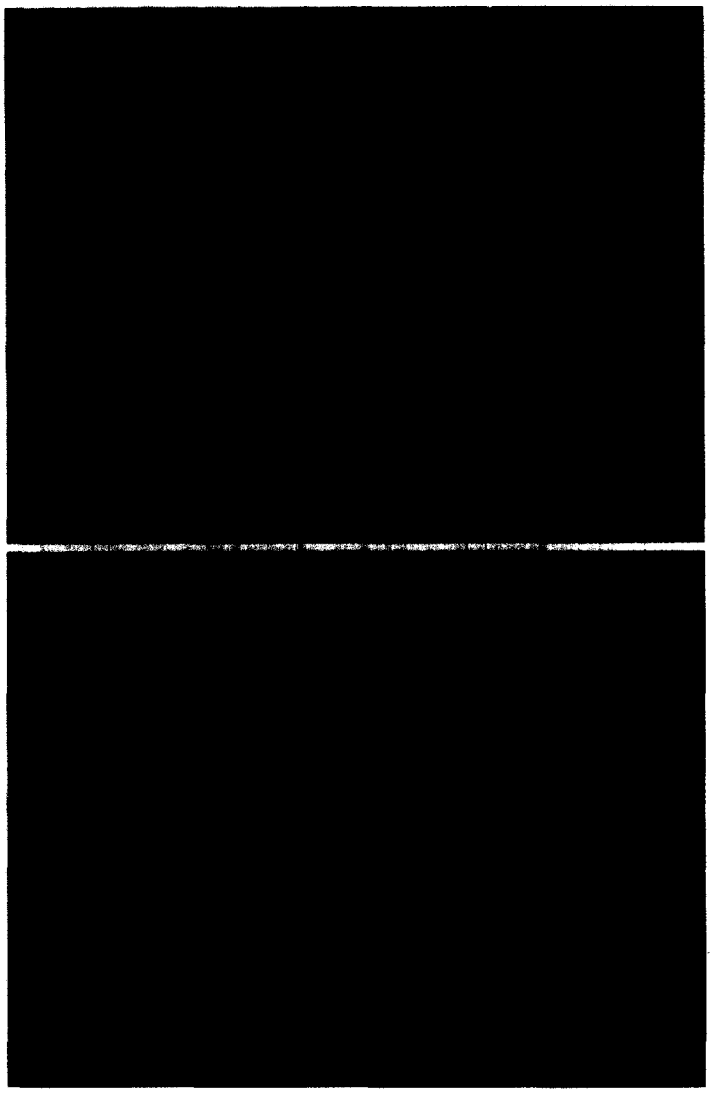

Fig. 8. Plasma density and magnetic field lines open (white) and closed (orange) before and after the arrival of the pressure filament. The black line represents the geosynchroneous orbit.

Acknowledgements. The authors would like to acknowledge the major contribution to this paper of A. Rodgers who compiled the outstanding collection of data for the March 9, 1995 substorm. Reprocessed WIND plasma and magnetic field data were provided by A. Lazarus and R. Lepping. Donation of computing resources by the Pittsburgh Supercomputer Center for the January 10–100 simulation is gratefully acknowledged. Work supported by NASA NAG5–1101.

References

Akasofu, S. I., *Polar and Magnetospheric Substorms*, D. Reidel, Hingham, MA, 1968.

Coroniti, F. V., and C. F. Kennel, Can the ionosphere regulate magnetospheric convection?, *J. Geophys. Res.*, *78*, 2837, 1973.

Fedder, J. A., and J. G. Lyon, The earth's magnetosphere is 165 R_E long: long or self-consistent currents, convection, magnetospheric structure and processes for northward IMF, *J. Geophys. Res.*, *100*, 3623, 1995.

Lopez, R. E., and A. T. Y. Lui, A multi-satellite case study of the expansion of a substorm current wedge in the near-Earth magnetotail, *J. Geophys. Res.*, *95*, 8009, 1990.

Lopez, R. E., H. Spence, and C.-L. Meng, Simultaneous observations of the westward electroject and the cross-tail current sheet during substorms, In: Magnetospheric substorms, ed. by J. R. Kan, T. A. Potemra, S. Kokubun, and T. Iijima, Geophysical Monograph 64, AGU, Washington, 1991.

Lopez, R. E., C. C. Goodrich, M. Wiltberger and J. G. Lyon, Simulation of the March 9, 1995 substorm and initial comparison to data, submitted to proceedings of "Ecounter Between Global Observations and Models in the ISTP Era (Huntsville '96)", (in press), March, 1997.

Lui, A. T. Y., A. Mankofsky, C. L. Chang, K. Papadopoulos, and C. S. Wu, A current disruption mechanism in the neutral sheet: a possible trigger for substorm expansions, *Geophys. Res. Lett.*, *17*, 745, 1990.

Lyon, J. G., and J. A. Fedder, Global simulation of a southward turnign of the IMF and its comparison with substorm morphology, submitted to *J. Geophys. Res.*, 1997.

Papadopoulos, K., A. S. Sharma, and J. A. Valdivia, Is the magnetosphere a lens for MHD waves? *Geophys. Res. Lett.*, *20*, 2809, 1993.